Plasma Science and Technology

On the electron sheath theory and its applications in plasma-surface interaction

To cite this article before publication: Guangyu Sun *et al* 2022 *Plasma Sci. Technol.* in press https://doi.org/10.1088/2058-6272/ac6aa7

On the electron sheath theory and its applications in plasma-surface interaction

Guangyu SUN (孙光宇)*, Zhang SHU (张舒)†, Anbang SUN (孙安邦)‡, and Guanjun ZHANG (张冠军)§

State Key Laboratory of Electrical Insulation and Power Equipment, School of Electrical Engineering, Xi'an Jiaotong University, Xi'an 710049, People's Republic of China

Abstract

In this work, an improved understanding of electron sheath theory is provided using both fluid and kinetic approaches while elaborating on their implications for plasma-surface interaction. A fluid model is proposed considering the electron presheath structure, avoiding the singularity in electron sheath Child-Langmuir law which overestimates the sheath potential. Subsequently, the kinetic model of electron sheath is established, showing considerably different sheath profiles in respect to the fluid model due to non-Maxwellian electron velocity distribution function and finite ion temperature. The kinetic model is then further generalized involving a more realistic truncated ion velocity distribution function. It is demonstrated that such distribution function yields a super-thermal electron sheath whose entering velocity at sheath edge is greater than the Bohm criterion prediction. Furthermore, an attempt is made to describe the electron presheath-sheath coupling within the kinetic framework, showing a necessary compromise between realistic sheath entrance and the inclusion of kinetic effects. Finally, the

* Current address: Ecole Polytechnique Fédérale de Lausanne, Swiss Plasma Center, CH-1015 Lausanne, Switzerland
† Current address: Laboratoire de Physique des Plasmas, Ecole Polytechnique, 91120 Palaiseau, France
‡ E-mail: anbang.sun@xjtu.edu.cn
§ E-mail: gjzhang@xjtu.edu.cn

secondary electron emissions induced by sheath-accelerated plasma electrons in electron sheath are analyzed, the influence of backscattering is discussed as well.

Keywords: plasma-surface interaction, sheath, secondary electron emission, Child-Langmuir law

(Some figures may appear in colour only in the online journal)

1. Introduction

The sheath is a space charge region commonly formed in the edge of plasma which breaks up the quasi-neutrality and shields the bulk plasma from solid boundary. Sheath plays essential role in confined plasma research, and in particular the plasma-surface interaction, such as plasma processing, plasma propulsion engine, magnetic-confined fusion, dust particles, plasma diagnostics, etc [1–9]. A classic Debye sheath (also called ion sheath) appears when a floating slab is injected into a plasma. Initially, more electrons than ions enter the board due to their higher mobility, leaving net positive charges in the gradually formed “sheath” region while depositing negative charges on the solid material, which in turn mitigates the electron flow until plasma current is balanced at the solid wall.

Though the ion-rich sheath is most frequently encountered, a sheath can be electron-rich in some particular cases. One example is when an electrode is biased above plasma potential in Langmuir probe voltage scan, where an electron sheath instead of ion sheath is formed near the electrode at high biased voltage [10, 11]. The electron sheath features the increasing potential from the sheath edge to the solid boundary, thus plasma electrons are accelerated by sheath potential whereas the ions are deaccelerated, contrary to the ion sheath. The electron sheath is a relatively local phenomenon, which requires concomitant ion sheath to present in other plasma-facing components to achieve the global particle balance in a confined plasma system [12]. If the surface areas where electron and ion sheath presents are noted as A_{w} and A_{e}, with

subscript w and c representing the electrode and other chamber wall, then the total electron current to all surfaces becomes $I_{\mathrm{e,tot}} = e\Gamma_{\mathrm{ep}}\left[A_{\mathrm{w}} + A_{\mathrm{c}}\exp\left(-\frac{e\varphi_{\mathrm{pc}}}{T_{\mathrm{ep}}}\right)\right]$. Here Γ_{ep} is the electron flux at sheath edge and φ_{pc} is the potential difference between other chamber wall and plasma (not between the electrode and plasma), which is positive. Total ion flux is $J_{\mathrm{i,tot}} = e\Gamma_{\mathrm{i}}A_{\mathrm{c}}$, with Γ_{i} the ion flux at sheath edge. The ion flux reaching the electrode where electron sheath presents is neglected due to limited ion temperature. Assuming Maxwellian electron and ion sheath Bohm criterion, the ion and electron current balance gives [13]:

$$e\varphi_{\mathrm{pc}} = -T_{\mathrm{ep}}\ln\left(\sqrt{\frac{2\pi m_{\mathrm{e}}}{m_{\mathrm{i}}}} - \frac{A_{\mathrm{w}}}{A_{\mathrm{c}}}\right) \tag{1}$$

Here m_{i} and m_{e} are ion and electron mass, respectively. The equation is similar to the floating sheath (with zero net current) potential expression except the $-\frac{A_{\mathrm{w}}}{A_{\mathrm{c}}}$ term. Equation (1) also requires that $A_{\mathrm{w}} \le A_{\mathrm{c}}\sqrt{\frac{2\pi m_{\mathrm{e}}}{m_{\mathrm{i}}}}$ which stipulates a limited surface area where electron sheath presents, i.e. an electron sheath cannot be floated since it requires ion sheath to appear elsewhere to achieve the global particle balance, and its existence is related to the area ratio between the total ion loss surface and the electrode surface near which electron sheath is formed [13].

Apart from the Langmuir probe sweep in the electron saturation region, electron sheath also appears in a variety of occasions in dusty plasma particle circulation, scrape-off layer diagnostics, planet surface, spacecraft probe, anode ablation by arc, and some transient processes [14–17]. Nonetheless, the related studies on electron sheath are far less than those of the ion sheath, and the electron sheath counterparts of some well-developed modeling in ion sheath have yet to be established.

Current study of electron sheath is primarily motivated by the pragmatic demand for probe diagnostics. For simplicity, a probe biased more positively than the plasma is assumed to collect

the full electron current from the electron sheath, while ions are neglected in the sheath. The electron velocity distribution function (EVDF) of sheath entrance is trivially regarded as half-Maxwellian and no presheath structure is considered [18]. These assumptions greatly facilitate the implementation of electron sheath physics into probe calibration. However, recent progresses of electron sheath theories showed that the underlying physics is far from simple. Simulation of Yee *et al* proved that a presheath exists for electron sheath which accelerates the plasma electrons up to the thermal velocity at sheath entrance [19]. The presheath size for electron sheath is larger than ion presheath and extends deeply into the bulk plasma. Also, a comprehensive presheath theory was proposed by Brett *et al* based on fluid equations [20]. It was shown that electrons in presheath are mainly driven by the pressure gradient, and that the accelerated electrons give rise to fluctuations due to ion acoustic instabilities. Instabilities in electron sheath were also investigated experimentally by Stenzel *et al* [21, 22]. Additionally, the transition between electron sheath and ion sheath was reproduced in simulation by varying electrode bias potential [23]. The electron sheath can even be enclosed by an ion presheath by surrounding a metallic electrode with dielectric material [24].

So far, the existing electron sheath theories are mostly based on fluid model and mainly focus on the presheath region, while the sheath is only treated as a boundary condition. The fluid model can be applied in the presheath region where collisionality is sufficiently large to form a near-Maxwellian distribution. However, the scenarios in the electron sheath region are more complex. In the present manuscript, electron sheath theories in low temperature, low pressure, unmagnetized plasma are investigated attentively. First of all, the newly discovered electron entering velocity at sheath edge inevitably yields a truncated electron velocity distribution function at sheath entrance. The ion entering velocity in the ion sheath edge barely matters since initial ion energy is far lower than the ion sheath potential energy, whereas this is not the case in the electron sheath. In addition, the plasma electrons are accelerated by the sheath potential and collide on the electrode with greater energy compared with the electrons in ion

sheath, inducing secondary electron emission (SEE). This may alter the current balance since both emitted electrons and plasma electrons contribute to the measured current, yet such effect has drawn few attentions. The present work attempts to address these issues on a theoretical ground and discuss their pertinent implications in plasma-surface interactions.

The paper structure is given as follows. In section 2 the Child-Langmuir law for electron sheath is reviewed, and is compared with an updated fluid model of electron sheath. Section 3 provides a comprehensive kinetic modeling of electron sheath, involving electron and ion velocity distribution function and the influence of electron-ion temperature ratio. In section 4 the secondary electron emission caused by sheath accelerated electrons is implemented in the electron sheath model. Concluding remarks are given in section 5.

2. Fluid model of electron sheath

2.1. Review of Child-Langmuir model in electron sheath

Child-Langmuir law is widely used for the descriptions of high voltage sheath, i.e. plasma-facing electrode is strongly biased such that the sheath potential is much larger than electron temperature as well as the floating sheath potential. For high voltage ion sheath, the sheath potential is too high for plasma electrons to penetrate the sheath, therefore only ion density is counted in the sheath. Different from the matrix sheath model where a uniform ion density is assumed inside the sheath, the Child-Langmuir model considers the acceleration of ions in the sheath and the consequent decreasing ion density towards the boundary. The floating ion sheath approaches the Child law sheath when the electrode potential becomes increasingly negative. The ion sheath potential of a floating, non-emissive boundary can be easily obtained from the balance of electron and ion fluxes. Here the electron flux is $\Gamma_{\mathrm{ep}} = n_{\mathrm{se}}\sqrt{\frac{T_{\mathrm{ep}}}{2\pi m_{\mathrm{e}}}}\exp\left(\frac{e\varphi_{\mathrm{ish}}}{T_{\mathrm{ep}}}\right)$, with φ_{ish} the ion sheath potential and T_{ep} the plasma electron temperature, and the ion flux is

$\Gamma_{\mathrm{i}} = n_{\mathrm{se}}\sqrt{\frac{T_{\mathrm{ep}}}{m_{\mathrm{i}}}} = h_{\mathrm{i}} n_0 \sqrt{\frac{T_{\mathrm{ep}}}{m_{\mathrm{i}}}}$. h_{i} is the presheath plasma density drop and is approximately 0.61, n_0 is the bulk plasma density. Here the ions are assumed to be cold. The current balance hence gives:

$$e\varphi_{\mathrm{ish}} = -\frac{T_{\mathrm{ep}}}{2}\ln\left(\frac{\mu}{2\pi}\right) \tag{2}$$

with $\mu = m_{\mathrm{i}} / m_{\mathrm{e}}$, n_{se} the plasma density at sheath edge (quasi-neutrality is assumed), and ion sheath potential $\varphi_{\mathrm{ish}} < 0$. It is noted that by convention the potential at sheath edge is assumed 0. When raising the biased voltage (absolute value), the flux balance at electrode is no longer valid and a net current term J_{net} must be counted to compensate: $\Gamma_{\mathrm{i}} - \Gamma_{\mathrm{ep}} = \Gamma_{\mathrm{net}} = J_{\mathrm{net}} / e$. In the high voltage sheath limit, electron flux term is dropped and the Child-Langmuir law for ion sheath as well as potential distribution is derived as:

$$J_{\mathrm{net}} = \frac{4\varepsilon_0}{9x_{\mathrm{ish}}^2}\sqrt{\frac{2e}{m_{\mathrm{i}}}}\left(-\varphi_{\mathrm{ish}}\right)^{3/2} \tag{3}$$

$$\frac{x}{\lambda_{\mathrm{De}}} = \frac{0.79}{\sqrt{h_{\mathrm{i}}}}\left(\frac{-e\varphi_{\mathrm{ish}}}{T_{\mathrm{ep}}}\right)^{3/4} \tag{4}$$

where x_{ish} is ion sheath length and λ_{De} is electron Debye length. Detailed derivations are available in numerous references and are not to be repeated here [10, 12]. In the case of electron sheath, the potential relative to sheath edge is positive, electrons are accelerated while ions are deaccelerated, so the electron sheath is assumed to be ion-free. The Poisson equation is written as:

$$\frac{\mathrm{d}^2\varphi}{\mathrm{d}x^2} = \frac{J_{\mathrm{net}}}{\varepsilon_0}\left(\frac{2e\varphi}{m_{\mathrm{i}}}\right)^{-0.5} \tag{5}$$

with ε_0 the vacuum permittivity, $J_{\text{net}} = en_{\text{ep}}(\varphi)\left(\frac{2e\varphi}{m_{\text{e}}}\right)^{0.5}$. In the case of a virtual anode between the plasma and electron sheath, $n_{\text{ep}} = n_0 h_{\text{e}} = n_0 \exp\left(-\frac{e\Delta\varphi}{T_{\text{ep}}}\right)$, with $\Delta\varphi$ the potential dip of virtual anode. For a highly emissive cathode a similar virtual cathode appears [25]. Multiplying both sides in equation (5) by $\frac{\mathrm{d}\varphi}{\mathrm{d}x}$ and integrating from the sheath edge to position x in the electron sheath, the following expression is obtained:

$$\frac{\mathrm{d}\varphi}{\mathrm{d}x} = \sqrt{\frac{4J_{\text{net}}}{\varepsilon_0}\left(\frac{m_{\text{i}}}{2e}\right)^{0.5}}\,\varphi^{0.25} \tag{6}$$

The potential and electric field are assumed 0 at sheath edge in deriving equation (6). Integrating above equation again and normalizing the x coordinate with regard to the electron Debye length λ_{De}, the Child-Langmuir law of electron sheath and potential distribution are derived with the current expression $J_{\text{net}} = en_{\text{se}}v_{\text{the}}$ as follows:

$$J_{\text{net}} = \frac{4\varepsilon_0}{9x_{\text{esh}}^2}\sqrt{\frac{2e}{m_{\text{e}}}}\left(\varphi_{\text{esh}}\right)^{3/2} \tag{7}$$

$$\frac{x}{\lambda_{\text{De}}} = \frac{0.79}{h_{\text{e}}}\left(\frac{e\varphi_{\text{esh}}}{T_{\text{ep}}}\right)^{3/4} \tag{8}$$

Same as equation (4), same conclusion was also reported by Brett *et al* [20]. A slightly different expression $\frac{x}{\lambda_{\text{De}}} = 0.32\left(\frac{e\varphi_{\text{esh}}}{T_{\text{ep}}}\right)^{3/4}$ was reported previously using different random flux expression [10].

An important assumption on the deduction above is the zero initial electron velocity at sheath edge. The ion velocity at sheath edge, in high voltage ion sheath, is commonly negligible when deriving the Child-Langmuir law, since the sheath potential is much larger than the electron temperature. As discussed in section 1, the electron presheath is not considered by the

conventional electron sheath theory. It was only recently that attention has been drawn regarding the importance of presheath in electron sheath properties [20, 26]. Electron entering velocity at sheath edge was shown to be $\sqrt{m_\mathrm{i}/m_\mathrm{e}}$ times larger than the ion Bohm velocity. Meanwhile, the electrode biased voltage is usually smaller in electron sheath compared with ion sheath in typical plasma applications. The treatment of electron entering velocity will be discussed in section 2.2, where it will be shown that such revision actually brings remarkable influence in the obtained sheath properties.

Another issue of the above deductions is the neglected electron velocity distribution function. Equation (4) implicitly regards electrons as monoenergetic beam. Though this is also used in the derivation of ion sheath Child-Langmuir law, one must realize that the electron temperature is far greater than ion temperature for a typical cold plasma discharge, thus the omission of electron kinetic effects in an electron sheath will introduce larger discrepancies compared with the neglection of IVDF in ion sheath. Further discussion on the treatment of EVDF will be given in section 3.

2.2. Revised fluid model of electron sheath

In this section, the electron sheath fluid model considering electron presheath is introduced. The derivation below is based on previous studies of the electron entering velocity in the electron sheath, but different conclusion of electron sheath structure is obtained, due to distinct treatment of Poisson equation [20]. To include the influence of electron entering velocity, it is intuitive to write down the electron fluid equations in sheath and regard the entering velocity as a boundary condition. To begin with, the particle and momentum balance of electron in sheath is given as follows:

$$\frac{\mathrm{d}}{\mathrm{d}x}\left(n_{\mathrm{ep}}u_\mathrm{e}\right)=0 \tag{9}$$

$$\frac{\mathrm{d}}{\mathrm{d}x}\left(m_{\mathrm{e}}n_{\mathrm{ep}}u_{\mathrm{e}}^2+P_{\mathrm{e}\|}\right)=-en_{\mathrm{ep}}E \tag{10}$$

In above equation, u_{e} is the electron fluid velocity, $P_{\mathrm{e}\|}$ is the parallel electron pressure, and E is the electric field. In equation (10), the pressure gradient force dominates over the electric field force, their ratio equals to the electron ion temperature ratio $T_{\mathrm{ep}}/T_{\mathrm{i}}$, obtained by inserting the ion momentum equation. For ion sheath it is the opposite, so that the pressure gradient can sometimes be ignored in fluid modeling [27, 28]. Similar conclusion was reported before [20]. Source terms are neglected since the sheath is assumed to be collisionless. Combining equations (9) and (10), and solving for u_{e} with potential φ, the following relation is obtained:

$$\int_{u_{\mathrm{eo}}}^{u_{\mathrm{e}}}\left(u'_{\mathrm{e}}-\frac{T_{\mathrm{ep}}}{m_{\mathrm{e}}u'_{\mathrm{e}}}\right)\mathrm{d}u'_{\mathrm{e}}=\frac{e}{m_{\mathrm{e}}}\int_0^{\varphi}\mathrm{d}\varphi' \tag{11}$$

where u_{eo} is the electron fluid velocity at sheath edge and is treated as the boundary condition, also the potential at sheath edge is chosen as 0. It is noted that here the temperature gradient term is dropped, and the isothermal relation is adopted. The resulting equation is:

$$\frac{1}{2}\left(\frac{u_{\mathrm{e}}}{u_{\mathrm{e}0}}\right)^2-\ln\left(\frac{u_{\mathrm{e}}}{u_{\mathrm{e}0}}\right)-0.5=\frac{e\varphi}{T_{\mathrm{ep}}} \tag{12}$$

Equation (12) can be solved by rewriting it in the form of Lambert W function and taking the asymptotic limit at large potential. More details on the solution of this form of equation were given in the work of Brett *et al* [20], here the result is given directly:

$$u_{\mathrm{e}}=u_{\mathrm{e}0}\sqrt{1+2e\varphi/T_{\mathrm{ep}}} \tag{13}$$

It is then possible to solve the Poisson equation in the following form:

$$\frac{\mathrm{d}^2\Phi}{\mathrm{d}X^2}=\left(1+2\Phi\right)^{-0.5} \tag{14}$$

Here the electron continuity equation ($n_{\mathrm{se}}u_{\mathrm{e}0}=n_{\mathrm{e}}u_{\mathrm{e}}$) is used again and the following normalized terms are adopted for simplicity.

$$\Phi = \frac{e\varphi}{T_{ep}}, X = \frac{x}{\lambda_{De}} \tag{15}$$

The potential distribution in electron sheath is then obtained by multiplying equation (14) by $\frac{d\Phi}{dX}$ and integrating twice with respect to X, which is reduced to:

$$X = \frac{\sqrt{2}}{6}\left(2\sqrt{2\Phi+1}+4\right)\sqrt{(2\Phi+1)^{0.5}-1} \tag{16}$$

The potential distributions given by equation (8), (16) and previous solution in reference [20] are shown in Figure 1 (named separately as the Child-Langmuir model which is the same as solution in reference [20], and the revised fluid model). Generally, the Child-Langmuir solution slightly overestimates the electron sheath potential.

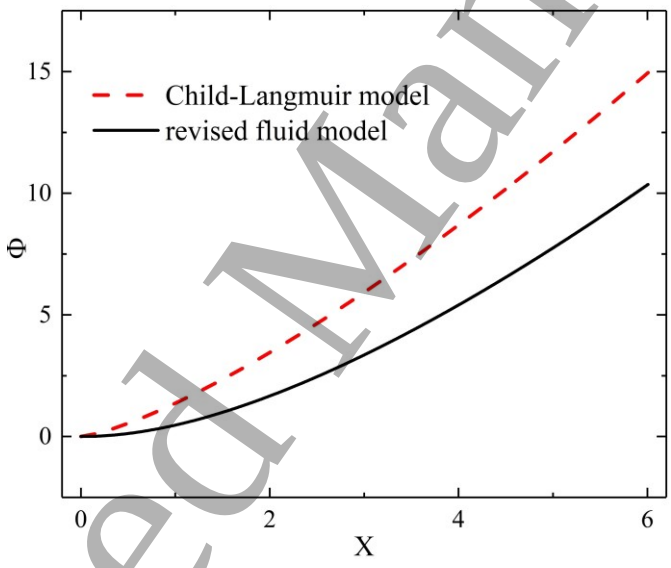

Figure 1. Comparison of potential distribution in electron sheath based on Child-Langmuir law and revised fluid model. Φ is normalized potential and X is normalized position. The Child-Langmuir model overestimates the sheath potential.

The electron density distributions in the sheath predicted by Child-Langmuir model and revised fluid model are shown in Figure 2. The Child-Langmuir model generally underestimates the electron density in locations far away from the sheath edge. One major flaw of Child-Langmuir model is that there exists a density singularity at $X = 0$ due to the neglection of

electron entering velocity at sheath edge. Section 3.1 will show that the singularity can also be avoided by considering electron kinetic effects even without involving the electron entering velocity at the sheath edge.

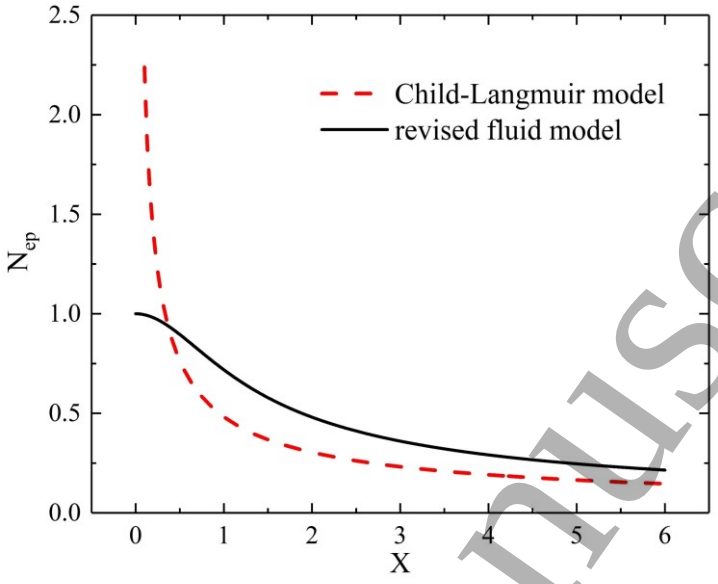

Figure 2. Normalized electron density distribution in sheath region predicted by Child-Langmuir model and revised fluid model. Child-Langmuir model gives infinite density at $X = 0$. The part of Child-Langmuir solution curve in the vicinity of singularity is not shown for better figure scaling. The Child-Langmuir law predicts lower electron density except near $X = 0$.

It is also important to point out that the obtained conclusions from equation (16) seem to be independent from the exact value of the entering velocity. This does not mean that the value of u_{e0} is irrelevant, rather it is just because the electron sheath cannot achieve self-consistency isolated from the presheath. For instance, the $u_{e0} = 0$ assumption adopted in Child-Langmuir solution will lead to unphysical solution of $u_e = 0$ everywhere according to equation (13). The $u_{e0} = 0$ assumption also leads to a singularity at sheath edge. Since the plasma electron flux conserves in the collisionless electron sheath, a zero entering velocity naturally causes infinite density at sheath entrance. Hence the inclusion of electron entering velocity is crucial. In addition, the choice of u_{e0} is not arbitrary, which is essentially dictated by the way the presheath

matches the sheath. Section 3.2 will show that the entering velocity can always be expressed in the form of $u_{e0} = \alpha_{ue0}\sqrt{\frac{T_{ep}}{m_e}}$ with α_{ue0} a coefficient depending on the electron and ion model (fluid or kinetic), their temperatures, and the choice of distribution function if kinetic model is employed. But at given model and plasma parameters, the value of u_{e0} is definite.

3. Kinetic model of electron sheath

3.1. Kinetic model without presheath

In section 2, the electron fluid equations are used to derive the electron sheath solution. However, the exact EVDF inside the sheath is not thoroughly considered. To illustrate the influence of kinetic effects on the electron sheath solution, the following kinetic model of electron sheath is constructed. In addition, ion velocity distribution function is involved to investigate the influence of nonzero ion temperature for more general applications of the theory.

To begin with, the electron and ion densities inside the sheath should be determined. The electrons are accelerated due to increasing sheath potential towards the electrode, hence a velocity lower bound appears when integrating the half-Maxwellian EVDF, which gives the following electron density:

$$n_{ep} = n_{se}\exp\left(\frac{e\varphi}{T_{ep}}\right)\operatorname{erfc}\left(\sqrt{\frac{e\varphi}{T_{ep}}}\right) \tag{17}$$

The ions are repelled by the electron sheath potential just as the electrons in an ion sheath. If the force posed by the electric field is balanced by the pressure gradient force, the Boltzmann distribution could be used to derive the following ion density:

$$n_i = n_{se}\exp\left(-\frac{e\varphi}{T_{ei}}\right) \tag{18}$$

The Poisson equation can therefore be written as:

$$\frac{\mathrm{d}^2\Phi}{\mathrm{d}X^2} = \exp(\Phi)\operatorname{erfc}\left(\sqrt{\Phi}\right) - \exp\left(-\Theta_T\Phi\right) \tag{19}$$

with $\Theta_T = T_{ep}/T_i$ the ratio of electron and ion temperature. Different from equations (5) and (14), equation (19) cannot be solved fully analytically. A possible solution is to reduce equation (19) into the following form, and then solve it as an initial value problem (IVP) numerically:

$$\frac{\mathrm{d}\Phi}{\mathrm{d}X} = \sqrt{2}\left[\exp(\Phi)\operatorname{erfc}\left(\sqrt{\Phi}\right) - 1 + 2\sqrt{\frac{\Phi}{\pi}} + \exp\left(\Theta_T\Phi\right)\right]^{0.5} \tag{20}$$

The equation above is obtained again by multiplying equation (19) by $\frac{\mathrm{d}\Phi}{\mathrm{d}X}$ and integrating twice over $\mathrm{d}X$. To solve for the potential numerically, the electrode potential relative to sheath edge is given as the initial condition. The potential is then solved towards the sheath edge using numerical methods. Here the explicit Euler method is employed:

$$\Phi_{n+1} = \Phi_n + g(\Phi_n)\Delta X, n = 1, 2, 3\ldots \tag{21}$$

with $g(\Phi)$ the RHS of equation (20), and ΔX the position step size. The initial condition at electrode is the normalized electron sheath potential: $\Phi_1 = \Phi_w = \Phi_{esh}$. Φ_w is the normalized potential at electrode and will constantly appear in the following derivations.

Calculated results with different Φ_w values are shown in Figure 3(a) and are compared with the Child-Langmuir prediction and the fluid model with presheath. One can find that the sheath size given by the kinetic model is typically above that given by the Child-Langmuir solution for smaller electron sheath and is below the Child-Langmuir solution for larger electron sheath and higher electrode potential. Considering electron presheath makes the electron sheath potential smaller for fixed sheath size, leaving it always below the kinetic model prediction except at very high electrode potential levels. Profiles of sheath potential distribution in space are remarkably different. In general, kinetic model predicts a shorter sheath size at fixed electrode potential, and its space potential profile is higher than the Child-Langmuir solution.

The influence of ion temperature is shown in Figure 3(b). It is clear that the ion temperature only exerts minor influence on the shape of potential profile, and high ion temperature slightly decreases the size of electron sheath. The potential profile becomes virtually insensitive to ion temperature after the value of Θ_T exceeds around 5. Consequently, in typical low temperature plasma applications, the influence of ion temperature on potential distribution is marginal. The calculated electron and ion density distributions in sheath predicted by kinetic model are compared with the Child-Langmuir model in Figure 4. The electron and ion densities are normalized with respect to the sheath edge density:

$$N = \frac{n}{n_{se}} \tag{22}$$

Generally, the kinetic model gives lower electron density compared with Child-Langmuir model and the fluid model considering electron presheath, suggesting an overestimation of plasma density when using fluid models, the ion density is ignored in fluid models. The kinetic model without electron presheath (hence zero entering velocity) and the fluid model considering electron presheath avoids the singularity at $X = 0$. The electron density profile is barely influenced by the change of Θ_T, whereas the ion density profile changes remarkably with Θ_T. Here the ion Boltzmann distribution is adopted, whereas in practice, some energetic ions might penetrate the electron sheath and arrive at electrodes, which is increasingly obvious for low Θ_T. These ions will not return to plasma and inevitably leaves an IVDF dissipated at high velocity tail [29]. Also, the ion density could be slightly higher than electron density in the vicinity of sheath edge. This actually contradicts the general Bohm criterion, and is due to the neglection of electron presheath structure in the kinetic model. Further analyses regarding more accurate IVDF and the influence of electron presheath structure on sheath solution will be given in sections 3.2 and 3.3.

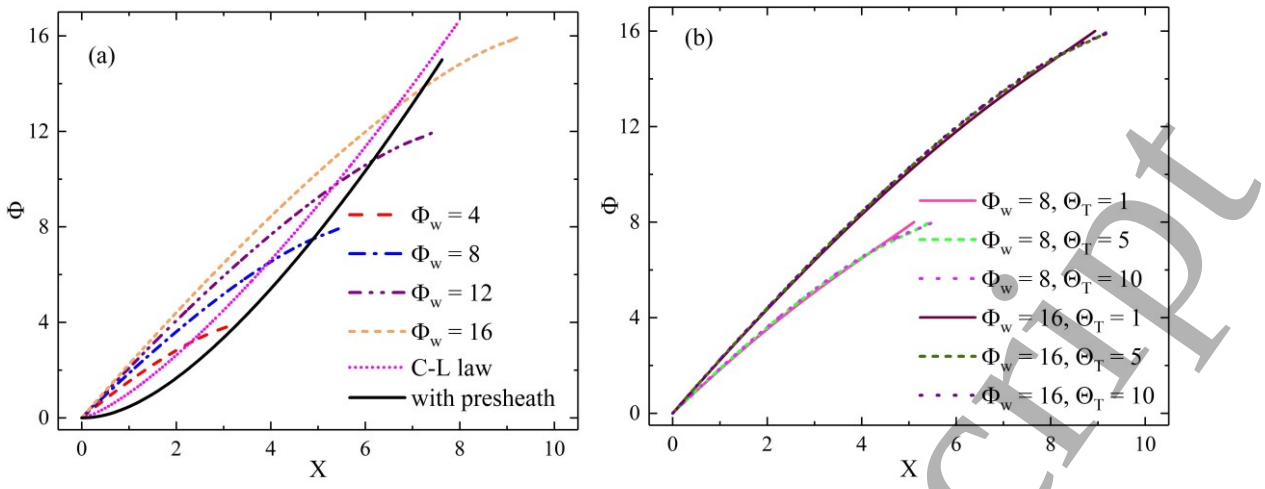

Figure 3. (a) The comparison of sheath potential distributions given by adopted kinetic model, Child-Langmuir law and fluid model with presheath. X is normalized position and Φ is normalized potential. (b) The influence of Electron-ion temperature ratio on sheath potential distribution. The influence is negligible after Θ_T surpasses 5.

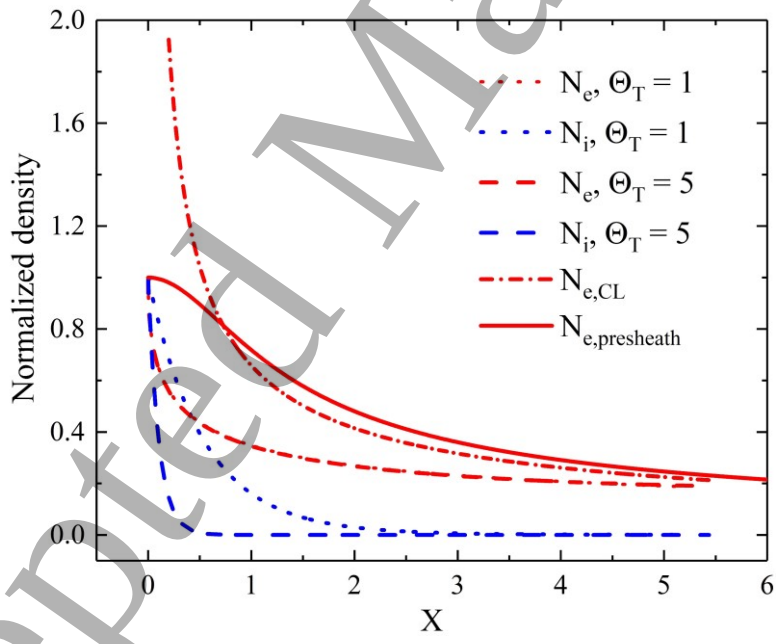

Figure 4. The electron and ion densities given by kinetic model, Child-Langmuir model and fluid model with electron presheath. Different electron-ion temperature ratios are used to illustrate influence of ion temperature. The part of Child-Langmuir solution curve in the vicinity of the singularity is not shown for better figure scaling. Electron density profile is not sensitive to Θ_T while ion density profiles change remarkably with Θ_T.

3.2. Derivation of Bohm criterion in electron sheath

In section 2, the influence of electron entering velocity on electron sheath solution has been illustrated, where the inclusion of electron fluid velocity u_{e0} as a boundary condition in sheath entrance shifts the size and potential distribution of the electron sheath. Judging solely from the sheath side, however, the value of u_{e0} seems arbitrary. In this section, the electron sheath will be matched with the presheath which dictates the choice of u_{e0}. The general Bohm criterion will first be applied in the electron sheath, then the modified Bohm criterion will be proposed considering more realistic IVDF. The obtained conclusions will be implemented into the following kinetic modeling of the electron sheath in various conditions.

3.2.1 Fluid derivation of Bohm criterion in electron sheath

The common procedure of the derivation of Bohm criterion for electron sheath is to calculate the electron and ion density at sheath edge and apply the general Bohm criterion, which is more universal and applies to both electron and ion sheath. The general Bohm criterion is frequently used directly and was originally proposed in Riemann's work [30]. However, sometimes its exact form could be vague in literatures and may cause misunderstanding when applied to ion and electron sheath. Here the general Bohm criterion is briefly reviewed and then directly applied to the case of electron sheath.

Starting from the Poisson equation and expand it at sheath edge:

$$\nabla^2\varphi = \frac{-1}{\varepsilon_0}\left[\rho\big|_{\varphi=0} + \frac{\mathrm{d}\rho}{\mathrm{d}\varphi}\bigg|_{\varphi=0}\varphi + \frac{\mathrm{d}^2\rho}{\mathrm{d}\varphi^2}\bigg|_{\varphi=0}\varphi^2 + \ldots\right] \tag{23}$$

with the charge density $\rho = e\left(n_\mathrm{i} - n_\mathrm{ep}\right)$. Taking up to first order in equation (23) and assuming quasi-neutrality at sheath edge, then multiplying with $\frac{\mathrm{d}\varphi}{\mathrm{d}x}$ and integrating over x, it leads to:

$$E^2 + \frac{1}{\varepsilon_0}\frac{\mathrm{d}\rho}{\mathrm{d}\varphi}\bigg|_{\varphi=0}\varphi^2 = C \tag{24}$$

where C is a constant to be determined. Since electric field is 0 at sheath edge, $C = 0$ and $\left.\frac{\mathrm{d}\rho}{\mathrm{d}\varphi}\right|_{\varphi=0}$ should satisfy:

$$\left.\frac{\mathrm{d}\rho}{\mathrm{d}\varphi}\right|_{\varphi=0} = -\left(\frac{E}{\varphi}\right)^2 \le 0 \tag{25}$$

Equation (25) can be further written as $\frac{\mathrm{d}\rho}{\mathrm{d}\varphi} = \frac{\mathrm{d}\rho}{\mathrm{d}x}\frac{\mathrm{d}x}{\mathrm{d}\varphi} = -E^{-1}\frac{\mathrm{d}\rho}{\mathrm{d}x} < 0$. It leads to the form of general Bohm criterion frequently used in literatures: $\frac{\mathrm{d}\rho}{\mathrm{d}x} > 0$ for ion sheath and $\frac{\mathrm{d}\rho}{\mathrm{d}x} < 0$ for electron sheath. Caution should be taken regarding the sign here.

With equation (25), the electron and ion density gradient at sheath edge is to be derived. To do that, electron and ion fluid equations in presheath are given as follows:

$$\frac{\mathrm{d}}{\mathrm{d}x}\left(n_\mathrm{i}u_\mathrm{i}\right) = S_\mathrm{ni} \tag{26}$$

$$\frac{\mathrm{d}}{\mathrm{d}x}\left(n_\mathrm{i}T_\mathrm{i}\right) = en_\mathrm{i}E + S_\mathrm{mi} \tag{27}$$

$$\frac{\mathrm{d}}{\mathrm{d}x}\left(n_\mathrm{ep}u_\mathrm{e}\right) = S_\mathrm{ne} \tag{28}$$

$$\frac{\mathrm{d}}{\mathrm{d}x}\left(m_\mathrm{e}n_\mathrm{ep}u_\mathrm{e}^2 + n_\mathrm{ep}T_\mathrm{ep}\right) = -en_\mathrm{ep}E + S_\mathrm{me} \tag{29}$$

where u_i is ion fluid velocity, S_ni, S_ne, S_mi and S_me are source terms for electron and ion particle and momentum balance. Comparing equations (27) and (29), one can find that the force on electrons contributed by electric field is roughly $\frac{T_\mathrm{i}}{T_\mathrm{ep}}$ times smaller than the pressure gradient term. Oppositely, it is the electric field that plays the dominant role in the ion-rich plasma sheath. Similar conclusions have been proposed by Brett *et al* [20]. At the sheath edge, the source terms near sheath edge are discarded and the ion and electron density gradients are obtained as follows:

$$\frac{\mathrm{d}n_\mathrm{i}}{\mathrm{d}x} = \frac{en_\mathrm{i}E}{T_\mathrm{i}} \tag{30}$$

$$\frac{\mathrm{d}n_\mathrm{ep}}{\mathrm{d}x} = \frac{en_\mathrm{ep}E}{m_\mathrm{e}u_\mathrm{e}^2 - T_\mathrm{ep}} \tag{31}$$

It is noted that $n_\mathrm{ep} = n_\mathrm{i}$ at sheath edge. Using equation (25), the Bohm criterion for electron sheath is derived as follows:

$$u_\mathrm{e}\big|_{\text{sheath edge}} = u_{\mathrm{e}0} \geq \sqrt{\frac{T_\mathrm{ep} + T_\mathrm{i}}{m_\mathrm{e}}} \tag{32}$$

Equation (32) is analogous to Bohm criterion for ion sheath except that electron entering velocity is $\sqrt{\frac{m_\mathrm{i}}{m_\mathrm{e}}}$ times larger than ion entering velocity.

3.2.2 Role of kinetic ions on Bohm criterion in electron sheath

In the deductions above, ions are assumed to be balanced by pressure gradient and electric field just as plasma electrons in an ion sheath. Actually, the EVDF in an ion sheath is commonly known as being depleted at high velocity end, since energic electrons that penetrate the ion sheath will not return to plasma. This phenomenon is known as the electron loss cone [31]. Generally speaking, the loss cone is a 3D phenomenon where electron velocity forms a spherical shell of radius $w = \frac{1}{2}m_\mathrm{e}\left(v_x^2 + v_y^2 + v_z^2\right)$ with w the electron energy. Electron with $w > e\Delta\varphi$ can have sufficient energy of motion normal to the wall (here in x direction) to leave the system, with $\Delta\varphi$ the wall-plasma potential difference [31]. In the present analyses, we focus on 1D1V model and only consider electron motion normal to the wall. The effects of depleted EVDF at high velocity tail in ion sheath due to loss cone effect have been addressed in detail by numerous works [32–34]. Particularly, Joaquim *et al* showed that the Bohm velocity of an ion sheath could be smaller than the conventional ion sound velocity $\sqrt{\frac{T_\mathrm{ep} + T_\mathrm{i}}{m_\mathrm{i}}}$ when the electron loss cone is considered [35]. Following a similar logic, it is intuitive to imagine that

the Bohm velocity of the electron sheath u_{e0} could also be affected by IVDF depleted at high velocity end, though the influence can only be obvious at high ion temperature.

Similar to the loss cone in the ion sheath, fast ion may penetrate the potential barrier in electron sheath and thus will not return, leading to the following truncated velocity distribution function:

$$f_i = n_i(\varphi)\begin{cases} \dfrac{1}{I(\eta)}\sqrt{\dfrac{m_i}{2\pi T_i}}\exp\left(-\dfrac{m_i v_i^2}{2T_i}\right), -\infty \le v_i \le v_{icut} \\ 0, v_i \ge v_{icut} \end{cases} \tag{33}$$

Here the normalized potential term is $\eta = \dfrac{e(\varphi_w - \varphi)}{T_i}$ with φ_w the potential at electrode (to be distinguished from Φ which is normalized with respect to T_{ep}), ion cutoff velocity is $v_{icut} = \sqrt{\dfrac{2e(\varphi_w - \varphi)}{m_i}} = \sqrt{2\eta}v_{thi}$, electrode potential relative to sheath edge is φ_w, and $I(\eta) = 0.5\left[1 + \mathrm{erf}\left(\sqrt{\eta}\right)\right]$. Ion flow velocity is then calculated as $u_i = \dfrac{v_{thi}}{I(\eta)}\exp(\Lambda - \eta)$, where ion thermal velocity is $v_{thi} = \sqrt{\dfrac{T_i}{m_i}}$ and $\Lambda = -\ln\left(\sqrt{2\pi}\right)$. Its derivation with respect to φ is $\partial_\varphi u_i = \dfrac{eu_i}{T_i}\left(1 + \dfrac{\exp(-\eta)}{2\sqrt{\pi\eta}I(\eta)}\right)$, to be used later on.

Above deductions solve the ion flux expression. Now equations (26), (28), (29) can be rewritten into the matrix form $MX = S$ with $X = (\partial_x n, \partial_x u_e, \partial_x \varphi)^T$, $S = (S_{ni}, S_{ne}, S_{me})^T$ and matrix M in the following form:

$$M = \begin{pmatrix} u_i & 0 & n\partial_\varphi u_i \\ u_e & n & 0 \\ T_{ep} & m_e n u_e & -en \end{pmatrix} \tag{34}$$

It is noted that in presheath the quasi-neutrality is satisfied so electron and ion densities are both n.

Since the gradient terms become much larger near sheath edge, it is assumed that $S=0$ and u_{e} is solved by using $|\mathrm{M}|=0$ in order to get a nontrivial set of solution, giving the following expression:

$$u_{\mathrm{e}}=\sqrt{\frac{T_{\mathrm{ep}}+T_{\mathrm{i}}/(1+\kappa)}{m_{\mathrm{e}}}}=u_{\mathrm{the}}\sqrt{1+\frac{T_{\mathrm{i}}}{T_{\mathrm{ep}}}\frac{1}{1+\kappa}} \tag{35}$$

with $\kappa=\dfrac{\exp(-\eta_{\mathrm{se}})}{2\sqrt{\pi\eta_{\mathrm{se}}}I(\eta_{\mathrm{se}})}$ (subscript se means sheath edge so $\eta_{\mathrm{se}}=\dfrac{e\varphi_{\mathrm{w}}}{T_{\mathrm{i}}}$) and electron thermal velocity $v_{\mathrm{the}}=\sqrt{\dfrac{T_{\mathrm{ep}}}{m_{\mathrm{e}}}}$. The electron entering velocity can be written as $u_{\mathrm{e0}}=\alpha_{\mathrm{ue0}}u_{\mathrm{the}}$, with the factor α_{ue0} in the following form:

$$\alpha_{\mathrm{ue0}}=\sqrt{1+\frac{1}{\Theta_{\mathrm{T}}}\frac{1}{1+\kappa}} \tag{36}$$

Above equation suggests that the electron sheath can become super-thermal, i.e. the electron entering velocity at sheath is higher than the thermal velocity predicted by Bohm criterion. Calculation results are shown in Figure 5(a). Clearly, electron flow velocity at sheath edge is always above the electron thermal velocity u_{the}, and increases with η_{SE}. It finally saturates at $v_{\mathrm{e,max}}=\sqrt{\dfrac{T_{\mathrm{ep}}+T_{\mathrm{i}}}{\mathrm{m_e}}}$ when $\eta_{\mathrm{SE}}\to\infty$. The influence of η_{SE} is actually unessential if Θ_{T} is large. Figure 5(a) also suggests that the presheath acceleration makes the drift velocity dominate the current, since the $u_{\mathrm{e0}}/v_{\mathrm{the}}$ is always above 1, constitutes a current at least around 2.5 times larger than the thermal flux without presheath. The presheath density drop could slightly reduce the difference of current values but the general trend is not changed. Meanwhile, ion flow velocity is always below its thermal velocity and decreases with η_{SE}.

One may also estimate ion heat flux $q_{\mathrm{i}}=\dfrac{1}{3}m_{\mathrm{i}}n_{\mathrm{i}}(v_x-u_{\mathrm{i}})^3$ by calculating v_x^2 and v_x^3 according to the distribution function in equation (33). Ion heat flux is expressed as follows:

$$q_{\mathrm{i}} = \frac{m_{\mathrm{i}} n_{\mathrm{i}} v_{\mathrm{thi}}^3}{\sqrt{2\pi} I(\eta)} \left[\exp(-\eta)\left(\eta - \frac{1}{2}\right) + \frac{3}{2}\sqrt{\frac{\eta}{\pi}}\frac{\exp(-2\eta)}{I(\eta)} + \frac{\exp(-3\eta)}{2\pi I^2(\eta)} \right] \tag{37}$$

It is noted that both v_{i} and q_{i} are independent from Θ_{T}. Calculation results are given in Figure 5(b) and (c). It is reasonable that the ion flux decreases with η_{SE} since a larger potential barrier obviously inhibits the ion flow in the electrons sheath, and the ion flux goes to 0 at infinite η_{SE}. The normalized electron sheath potential η_{SE} not only affects the ion energy drop when crossing the sheath, but also controls the ion velocity bound via v_{icut}. The resulting ion heat flux first increases and then decreases as η_{SE} increases. This indicates an ion erosion peak when an electrode is biased just above the plasma potential and should be avoided in practice. The trend is similar to the electron heat flux in a subsonic ion sheath and shows interesting symmetry between the two types of sheaths [35].

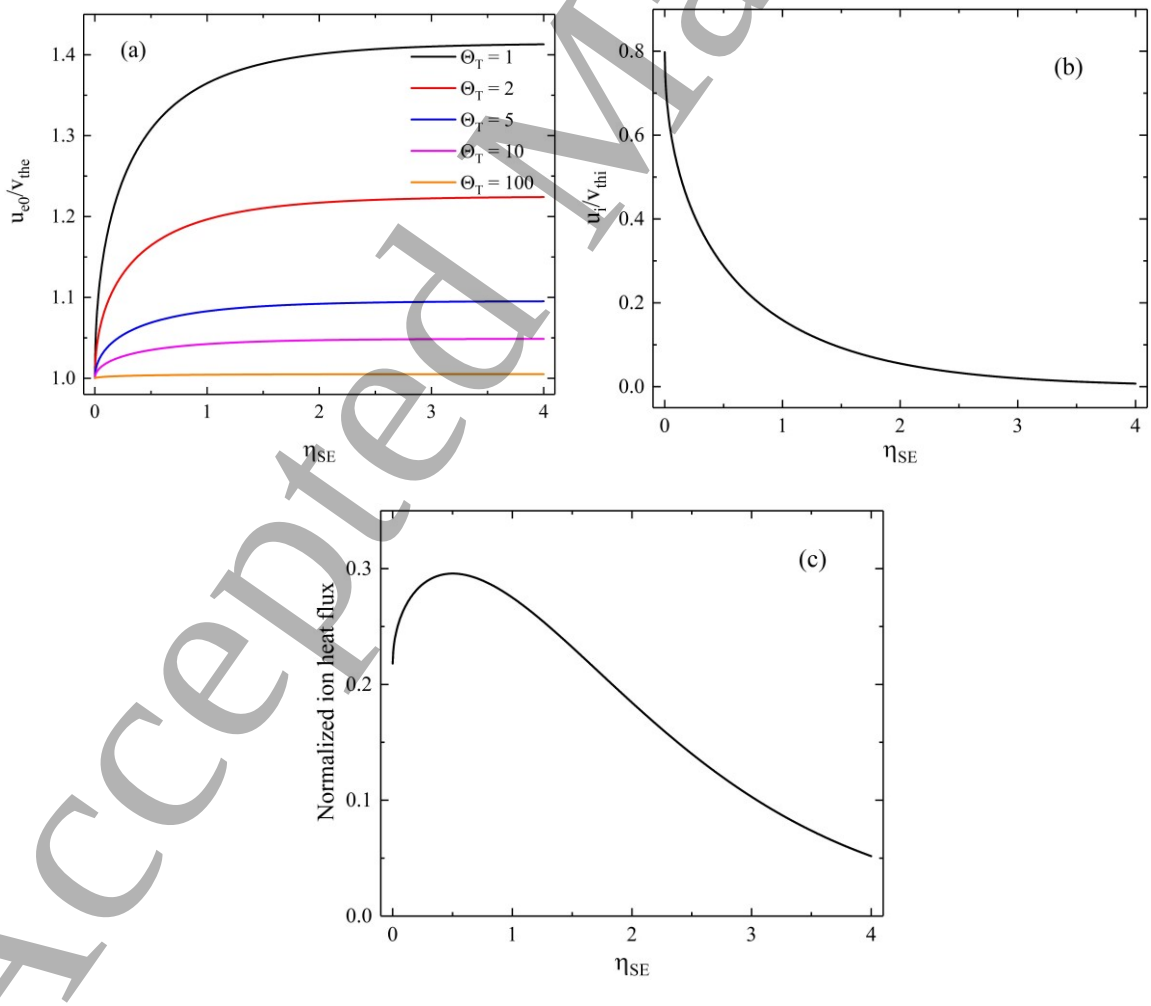

Figure 5. Sheath edge properties as function of term $\eta_{SE} = \frac{e\varphi_w}{T_i}$ and $\Theta_T = \frac{T_{ep}}{T_i}$. (a) Electron entering velocity at sheath edge normalized with respect to electron thermal velocity. Electron velocity increases with η_{SE} while its influence becomes smaller at higher Θ_T, (b) ion velocity normalized over ion thermal velocity, which decreases with η_{SE}, (c) ion heat flux normalized over $\frac{1}{2} m_i n_{SE} v_{th}^3$.

To summarize above, various forms of electron entering velocity are introduced in the section. When neglecting all ions, it is simply $u_{e0} = \sqrt{\frac{T_{ep}}{m_e}}$. If considering nonzero ion temperature while disregarding the ion loss cone, the expression becomes $u_{e0} = \sqrt{\frac{T_{ep} + T_i}{m_e}}$. If one further involves the ion loss cone, the entering velocity is expressed as $u_{e0} = \alpha_{ue0} u_{the}$, with $\alpha_{ue0} = \sqrt{1 + \frac{1}{\Theta_T} \frac{1}{1+\kappa}}$. Although the value of electron presheath potential (or u_{e0}) does not directly change the calculated electron sheath potential and plasma density profiles, a nonzero u_{e0} is necessary to avoid the electron density singularity for fluid model. In addition, the electron presheath structure is affected by the sheath parameters particularly the electron sheath potential, with the effect more obvious for high ion temperatures. These expressions will be used in the following derivations.

3.3. Application of Bohm criterion in kinetic model of electron sheath

3.3.1 Influence of truncated EVDF on kinetic model of electron sheath

In section 3.2, the electron entering velocity u_{e0} is derived with various types of assumption. It is then possible to apply the obtained u_{e0} to revise the EVDF at sheath entrance. Note that in section 3.1, the EVDF at sheath edge is in Maxwellian form and no drift velocity is considered.

When u_{e0} is included, however, the EVDF at sheath edge is inevitably truncated, and a drift velocity should be included.

For simplicity, the original EVDF is assumed to be a half-Maxwellian with no drift velocity, and then a nonzero u_{e0} is added to see its influence. The comparison of the EVDFs with and without entering velocity is given in Figure 6.

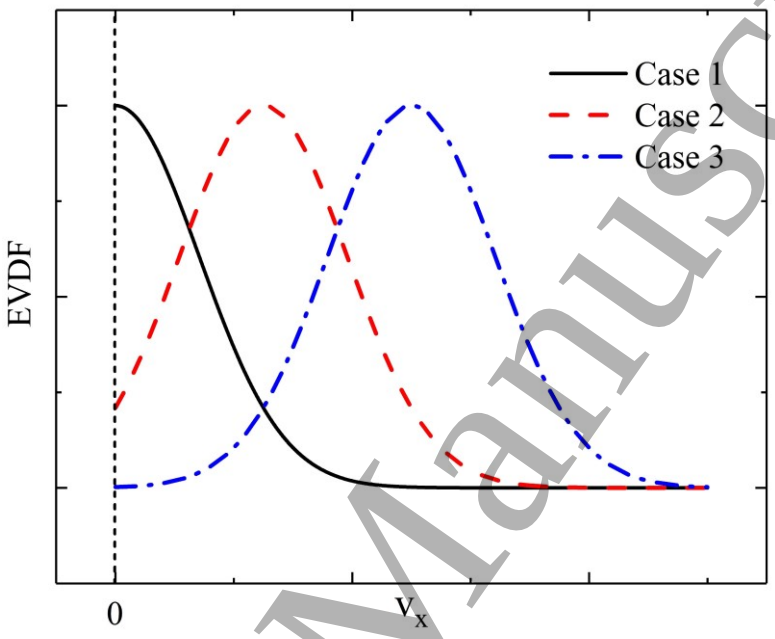

Figure 6. The schematic of the EVDFs with zero or nonzero entering velocity. EVDFs are normalized with respect to the density. Case 1 is the half-Maxwellian case, case 2 is an arbitrary nonzero entering velocity case, while case 3 is similar to case 2 except that the drift velocity is sufficiently large so that EVDF is close to a drifting Maxwellian.

The half-Maxwellian EVDF in Figure 6 is simply $f_{e,hM} = n_{se}\sqrt{\frac{2m_e}{\pi T_{ep}}}\exp\left(-\frac{m_e v_e^2}{2T_{ep}}\right)$. The truncated EVDFs in Figure 6 are as follows:

$$f_{e,ue0} = n_{se}\frac{1}{1+\mathrm{erf}\left(u_{e0}\sqrt{\frac{m_e}{2T_{ep}}}\right)}\sqrt{\frac{2m_e}{\pi T_{ep}}}\exp\left[-\frac{m_e\left(v_e-u_{e0}\right)^2}{2T_{ep}}\right], v_e \geq 0 \quad (38)$$

The additional factor in equation (38) compared with the half-Maxwellian is derived by normalization of the sheath edge density n_{se}. When $u_{e0}=0$, equation (38) is reduced to the half-Maxwellian as used in section 3.1, whereas the EVDF approaches a flowing Maxwellian when u_{e0} is larger than the electron thermal velocity. This suggests that the fluid model employed in section 2.2 is an approximation of infinite electron entering velocity.

The electron flux at sheath edge is then calculated as:

$$\Gamma_{ep,ue0}=\int_0^{+\infty} v_e f_{e,ue0}\mathrm{d}v_e=\beta_e\Gamma_{ep,hM} \tag{39}$$

where $\Gamma_{ep,hM}=n_{se}\sqrt{\frac{2T_{ep}}{\pi m_e}}$ is the electron flux at sheath edge for half-Maxwellian EVDF, and β_e is a coefficient depending on u_{e0}, shown as follows:

$$\beta_e=\frac{\exp\left(-\frac{m_e u_{e0}^2}{2T_{ep}}\right)}{1+\mathrm{erf}\left(u_{e0}\sqrt{\frac{m_e}{2T_{ep}}}\right)}+u_{e0}\sqrt{\frac{\pi m_e}{2T_{ep}}} \tag{40}$$

Equation (40) can be justified by the limit $u_{e0}=0$ which yields $\beta_e=1$ and is equivalent to the half-Maxwellian case. For typical low temperature plasma with $T_{ep}\gg T_i$, $u_{e0}=\sqrt{\frac{T_{ep}}{m_e}}$ and $\beta_e\approx 1.61$. Note that in section 3.2 the electron entering velocity is expressed as $u_{e0}=\alpha_{ue0}u_{the}$, where $u_{the}=\sqrt{\frac{T_{ep}}{m_e}}$ and α_{ue0} depends on the electron-ion temperature ratio Θ_T and $\kappa(\Phi_w)$. The calculated results of factor β_e are shown in Figure 7.

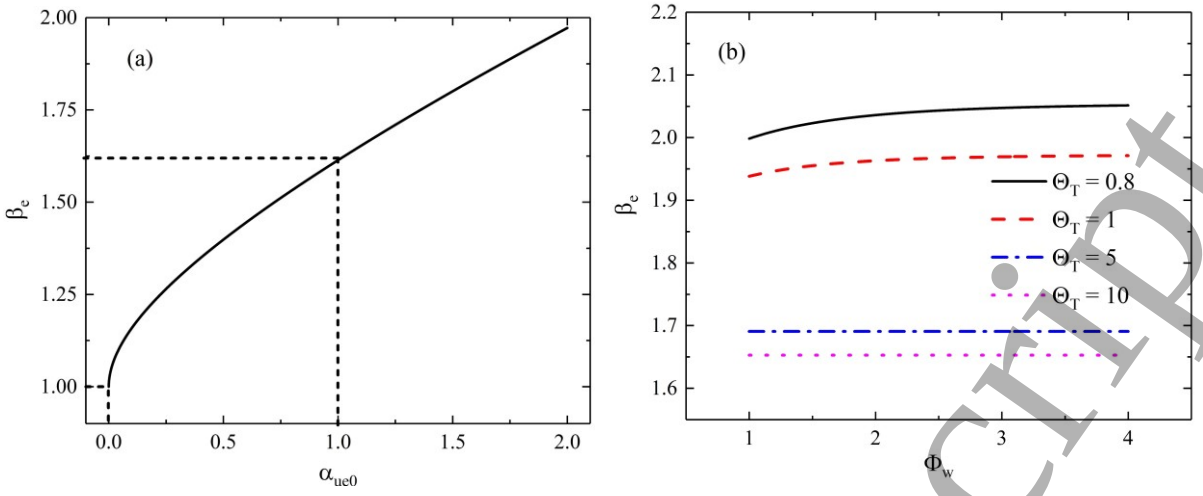

Figure 7. Calculated β_e as a function of (a) α_{ue0} and (b) Φ_w and Θ_T.

It is clear that the value of β_e increases with α_{ue0}. The presheath-sheath matching requires that $\alpha_{ue0} \in [1,2]$, which dictates a minimum β_e of around 1.61 and maximum of around 1.97. In Figure 7(b) one can find that the influence of Φ_w on β_e is obvious at low Θ_T levels, and the Θ_T plays more significant role compared with Φ_w. This is as expected because the ion loss cone is obvious only when sufficient amounts of ions can penetrate the electron sheath potential. At higher Θ_T level, the normalized electrode potential Φ_w is not influential. This is reassuring for low temperature plasma applications such as Langmuir probe, since if the entering velocity changes with electrode bias potential, the probe measurement must therefore be calibrated accordingly. However, for lower Θ_T ($\Theta_T < 1$), the influence of Φ_w is quite remarkable (not shown here), corresponding to, for instance, the plasma in divertor region of magnetic confinement fusion device [36]. This might rise concern for probe data processing in edge fusion plasma but is beyond the scope of the present work. Actually, the sheath physics and probe diagnostics in strongly magnetized fusion plasma are far more complex than the model considered here. First of all, the magnetic field typically interacts with the solid surface at an oblique angle, which produces a magnetic presheath with thickness of a few Larmor radii between the presheath and sheath [37]. In addition, the probe is subject to more complex plasma

environment such as perpendicular flow, multiple types of bias, etc [38]. Future experimental works in fusion background are expected to further address this issue.

3.3.2 An attempt to include Bohm criterion in the kinetic model of electron sheath

In section 3.1, a kinetic model is established for electron sheath involving the corrected EVDF at the sheath edge, which provides numerical solution of the sheath structure. However, the electron entering velocity is not counted in that model. It is therefore intuitive to consider if it is possible to modify the form of EVDF at sheath edge according to the revised electron Bohm criterion and apply similar methods to further improve the kinetic modeling. It will be shown in the following section that this is not as straightforward as anticipated, and not even a numerical solution could be obtained when the entering velocity is considered.

In an arbitrary position of the electron sheath, its EVDF should contain the drift velocity u_{e0} imposed by Bohm criterion and the electron cutoff velocity v_{ecut} due to field acceleration. It is noted that $u_{e0} = \alpha_{ue0} u_{the}$ and $v_{ecut} = \sqrt{2\Phi_w \frac{T_{ep}}{m_e}}$. In order to apply the similar methods in section 3.1, the electron density should be evaluated first. The integral of the EVDF depends on the relative position between u_{e0} and v_{ecut} in the velocity axis, as shown in figure 8.

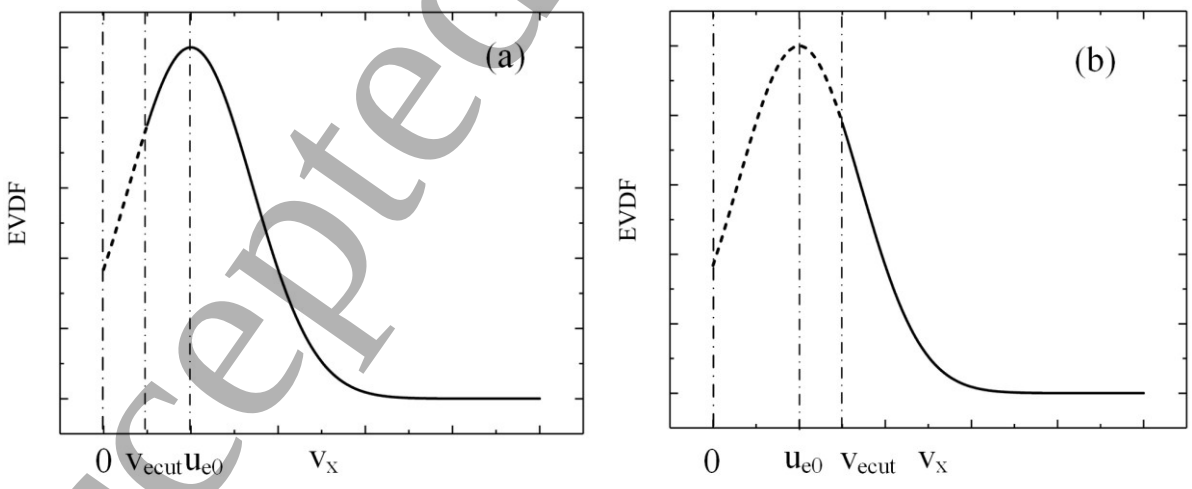

Figure 8. Schematic of two cases of EVDF and the influence of the relation between u_{e0} and v_{ecut}. The solid line marks the physical velocity distribution function.

In case 1 the electron density is calculated to be:

$$n_{\mathrm{ep1}} = n_{\mathrm{se}} \exp\left(\frac{e\varphi}{T_{\mathrm{ep}}}\right) \frac{1+\mathrm{erf}\left[\left(u_{\mathrm{e0}} - v_{\mathrm{ecut}}\right)\sqrt{\frac{m_{\mathrm{e}}}{2T_{\mathrm{ep}}}}\right]}{1+\mathrm{erf}\left(u_{\mathrm{e0}}\sqrt{\frac{m_{\mathrm{e}}}{2T_{\mathrm{ep}}}}\right)} \tag{41}$$

When $v_{\mathrm{ecut}} = 0$, $\varphi = 0$, which corresponds to the sheath edge, one arrives at $n_{\mathrm{ep}}\big|_{\mathrm{se}} = n_{\mathrm{se}}$. For case 2, the integrated electron density is in the following form:

$$n_{\mathrm{ep2}} = n_{\mathrm{se}} \exp\left(\frac{e\varphi}{T_{\mathrm{ep}}}\right) \frac{\mathrm{erfc}\left[\left(v_{\mathrm{ecut}} - u_{\mathrm{e0}}\right)\sqrt{\frac{m_{\mathrm{e}}}{2T_{\mathrm{ep}}}}\right]}{1+\mathrm{erf}\left(u_{\mathrm{e0}}\sqrt{\frac{m_{\mathrm{e}}}{2T_{\mathrm{ep}}}}\right)} \tag{42}$$

Here when $u_{\mathrm{e0}} = 0$, the expression is reduced to the equation (17) where no entering velocity is considered. Therefore, the two expressions above can be justified by the limits. Also, it is noted that the above two equations are continuous at $v_{\mathrm{ecut}} = u_{\mathrm{e0}}$.

However, when bringing the electron density expression into the Poisson equation, no analytical expression can be obtained from the integral of equations (41) and (42), so not even the numerical solutions of electron sheath, as in section 3.1, are derivable. This indicates that a compromise has to be made when choosing the electron sheath model: either the electron sheath Bohm criterion is counted and fluid model is employed (section 2.2) or the kinetic effects (EVDF) is considered while entering velocity must be dropped. Future works are expected to propose better solution and self-consistently combine the truncated EVDF and electron sheath solution.

4. Electron sheath modeling considering plasma-surface interaction

Secondary electron emission widely exists in a multitude of scenarios where plasma flux coming from sheath contacts the solid boundaries [31, 33, 34, 39, 40]. Both incident ion and electron can induce SEE at solid boundary. The former is generally through Auger neutralization or deexcitation where ion approaching the solid boundary bends the local field nearby so that the trapped electrons can escape from the solid material [41]. The latter happens when the incident primary electron is deaccelerated after penetrating the material surface while transferring energy to surrounding electrons, some of which could evacuate from material surface and become true secondary electrons [42].

In low temperature plasma applications, both types of SEE could happen, but not both of them are considered simultaneously in most if not all plasma simulations. The ion-induced SEE coefficient is independent from the incident ion temperature (only true for cold ion) and is a constant once the wall material is fixed. Recent theories showed that the accumulated surface charges in dielectric materials can modify the ion-induced SEE coefficient [43]. The present study focuses on metallic boundary, hence ion-induced SEE coefficient remains constant. On the other hand, the electron-induced SEE depends on primary electron energy. The ion-induced SEE is usually counted if the electron temperature is low and the wall material is metallic which has lower electron-induced SEE coefficient. Taking the example of plasma processing using capacitively-coupled plasma, it is usually the ion-induced SEE that is counted since electrodes are typically metallic and electron temperature is low [44], whereas the electron-induced SEE was shown to be influential if the neutral pressure is low and the electrodes are made of more emissive material such as SiO_2 [45].

In the particular case of the electron sheath, the reason why special attention is drawn towards electron-induced SEE is that the plasma electrons are accelerated by the sheath potential. The electron incident energy on electrode for an ion sheath is $2T_{ep}$, whereas the

incident energy for an electron sheath is $2T_{ep} + e\varphi_w$. This indicates the possible significance of electron-induced SEE (simply called SEE in the following section) even with metallic electrode.

To include SEE into electron sheath theory, it is important to first clarify the electron dynamics therein. The plasma electrons are accelerated, colliding on electrode and causing SEE. Emitted electrons are repelled by the sheath potential and some of them are returned to the electrode. Since the reflected emitted electron energy is usually much smaller than the energy of sheath-accelerated plasma electrons, it is assumed that the reflected electrons no longer cause SEE. The following derivations are inspired by the highly emissive inverse sheath model [46]. The inverse sheath is fundamentally different from the electron sheath discussed here, since it has no presheath and requires an electron emission coefficient greater than 1. The inverse sheath does not require strongly biased electrode and can appear on large, floating surface (no need for $A_w \ll A_c$). The electron fluxes at electrode for the electron sheath should satisfy the following equation:

$$\Gamma_{ep} + \Gamma_{eref} - \Gamma_{em} = \Gamma_{net} \tag{43}$$

where Γ_{eref}, Γ_{em}, and Γ_{net} are reflected electron flux, emitted electron flux and the net electron flux, respectively. Γ_{net} must be balanced with flux at other chamber surfaces where ion sheath presents.

The reflected electron flux is in the following form:

$$\Gamma_{eref} = \Gamma_{em}\left[1 - \exp\left(-\frac{e\varphi_w}{T_{em}}\right)\right] \tag{44}$$

Bringing in the definition of SEE coefficient $\gamma_e = \Gamma_{em}/\Gamma_{ep}$, the following equation can be derived:

$$\Gamma_{net} = \Gamma_{em}\left[\gamma_e^{-1} - \exp\left(-\frac{e\varphi_w}{T_{em}}\right)\right] \tag{45}$$

The expression of plasma electron flux at sheath edge is again $\Gamma_{ep} = n_{sep}\beta_e\sqrt{\frac{2T_{ep}}{\pi m_e}}$, here the plasma electron density at sheath edge n_{sep} is not equal to the sheath edge density n_{se}, since n_{se} contains both plasma electrons and emitted electrons. In addition, a strong surface emission can lead to formation of local potential dip which changes the density drop at the sheath edge. This effect is characterized by the factor $h_e = \exp\left(-\frac{e\Delta\varphi}{T_{ep}}\right)$ with $\Delta\varphi$ the local potential dip and is now not included in the present model for simplicity. Regarding the distribution function of emitted electrons, the half-Maxwellian is frequently chosen to facilitate the calculation, though it was also shown that the choice of EVDF for emitted electrons can bring some influences in sheath solution [47]. The emitted electron flux at electrode is simply calculated by the equation:

$$\Gamma_{em} = n_{emw}\sqrt{\frac{2T_{em}}{\pi m_e}} \tag{46}$$

with n_{emw} the emitted electron density at electrode. At sheath edge, the total electron density is summed up to be n_{se}, which gives the following equation:

$$n_{emw}\exp\left(-\frac{e\varphi_w}{T_{em}}\right) + n_{sep} = n_{se} \tag{47}$$

Combining the above equations, the following expression for electron sheath potential is derived:

$$\Gamma_{net} = n_{se}\sqrt{\frac{2T_{em}}{\pi m_e}}\frac{\gamma_e^{-1} - \exp\left(-\frac{e\varphi_w}{T_{em}}\right)}{\exp\left(-\frac{e\varphi_w}{T_{em}}\right) + \sqrt{\Theta_{Tem}}\left(\gamma_e\beta_e\right)^{-1}} \tag{48}$$

where $\Theta_{Tem} = T_{em}/T_{ep}$. The relation here is essentially *I-V* trace of the emissive electron sheath, which means that the electrode current is known once the applied bias potential φ_w is given. A change of the sheath *I-V* characteristic, if not considered in probe calibration, can influence the

measurement precision. The relation between applied electrode potential and electrode current can be further simplified as follows:

$$\Phi_{\mathrm{w}} = \Theta_{\mathrm{Tem}} \ln\left(\gamma_{\mathrm{e}} \frac{1+\xi}{1-\xi\sqrt{\Theta_{\mathrm{Tem}}}\beta_{\mathrm{e}}^{-1}} \right) \tag{49}$$

with Φ_{w} the normalized electrode potential, and the factor ξ a normalized term in the following form:

$$\xi = \frac{\Gamma_{\mathrm{net}}}{n_{\mathrm{se}}\sqrt{\dfrac{2T_{\mathrm{em}}}{\pi m_{\mathrm{e}}}}} \tag{50}$$

It has to be pointed out that the newly introduced factor ξ is not straightforward in physical meaning, but the denominator of RHS of equation (49) dictates a singularity at $1 = \xi\sqrt{\Theta_{\mathrm{Tem}}}\beta_{\mathrm{e}}^{-1}$ which is simplified as $\Gamma_{\mathrm{ep}} = \Gamma_{\mathrm{net}}$. According to equations (43) and (44), $\Gamma_{\mathrm{ep}} - \Gamma_{\mathrm{em}} \exp\left(-\dfrac{e\varphi_{\mathrm{w}}}{T_{\mathrm{em}}} \right) = \Gamma_{\mathrm{net}}$. Therefore, the singularity is never achieved as long as secondary electron emission exists. While the upper bound of possible ξ value is prescribed by this singularity, the lower bound of ξ should guarantee that $\Phi_{\mathrm{w}} \geq 0$ (ensure the existence of electron sheath). The calculation results given by equation (49) are shown in Figure 9.

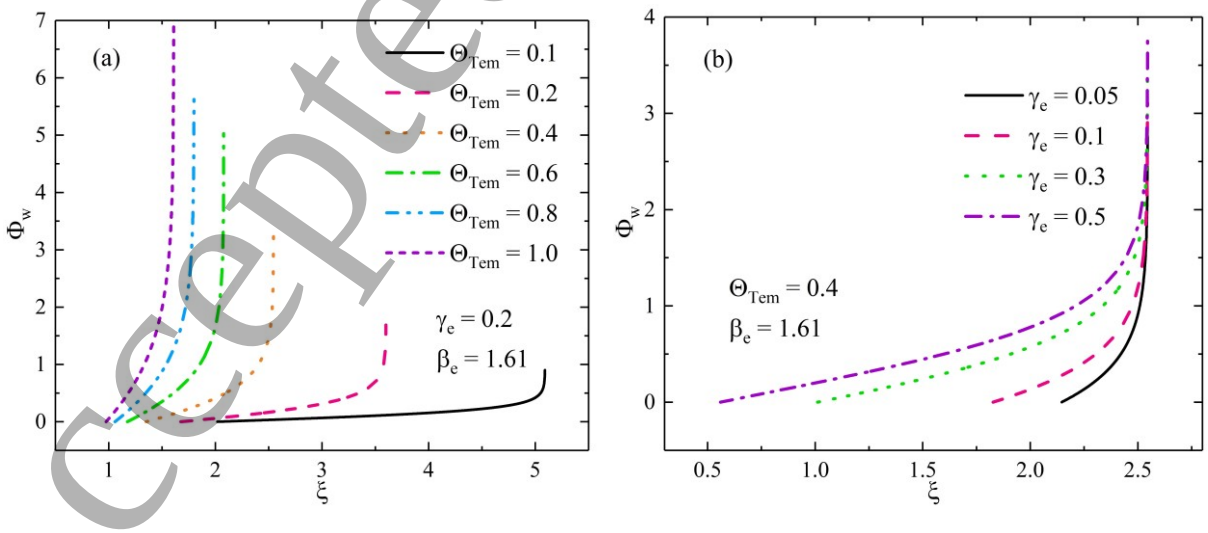

Figure 9. Calculated normalized electrode potential as function of ξ, γ_{e}, Θ_{Tem} and β_{e}.

It is obvious that the value of Θ_{Tem} has remarkable influence on the range of possible ξ. The value of β_{e} varies between around 1.61 and 1.97, hence posing fairly limited influence on the profile of Φ_{w} (not shown). The emission coefficient mainly changes the lower bound of ξ since a higher γ_{e} allows for smaller ξ value before the term $\gamma_{\mathrm{e}} \frac{1+\xi}{1-\xi\sqrt{\Theta_{\mathrm{Tem}}}\beta_{\mathrm{e}}^{-1}}$ reaches 1.

With equations (43)–(47), the two normalized electron densities $N_{\mathrm{sep}} = \frac{n_{\mathrm{sep}}}{n_{\mathrm{se}}}$ and $N_{\mathrm{emw}} = \frac{n_{\mathrm{emw}}}{n_{\mathrm{se}}}$, which represent normalized plasma electron density at sheath edge and emitted electron density at the electrode, can be expressed with given normalized electrode bias potential Φ_{w}:

$$N_{\mathrm{sep}} = \frac{n_{\mathrm{sep}}}{n_{\mathrm{se}}} = \frac{\sqrt{\Theta_{\mathrm{Tem}}}/\left(\gamma_{\mathrm{e}}\beta_{\mathrm{e}}\right)\exp\left(\frac{\Phi_{\mathrm{w}}}{\Theta_{\mathrm{Tem}}}\right)}{1+\sqrt{\Theta_{\mathrm{Tem}}}/\left(\gamma_{\mathrm{e}}\beta_{\mathrm{e}}\right)\exp\left(\frac{\Phi_{\mathrm{w}}}{\Theta_{\mathrm{Tem}}}\right)} \tag{51}$$

$$N_{\mathrm{emw}} = \frac{n_{\mathrm{emw}}}{n_{\mathrm{se}}} = \left[\exp\left(-\frac{\Phi_{\mathrm{w}}}{\Theta_{\mathrm{Tem}}}\right) + \sqrt{\Theta_{\mathrm{Tem}}}/\left(\gamma_{\mathrm{e}}\beta_{\mathrm{e}}\right)\right]^{-1} \tag{52}$$

Here γ_{e}, β_{e}, Θ_{Tem} are regarded as constant once bias potential is fixed. With equations (51) and (52), all electron density components in the electron sheath become functions of space potential:

$$N_{\mathrm{ep}} = N_{\mathrm{sep}}\exp\left(\Phi\right)\mathrm{erfc}\left(\sqrt{\Phi}\right) \tag{53}$$

$$N_{\mathrm{em}} = N_{\mathrm{emw}}\exp\left(\Phi - \Phi_{\mathrm{w}}\right) \tag{54}$$

$$N_{\mathrm{ref}} = N_{\mathrm{em}}\mathrm{erf}\left(\sqrt{\Phi/\Theta_{\mathrm{Tem}}}\right) \tag{55}$$

The Poisson equation is then:

$$\frac{\mathrm{d}^2\Phi}{\mathrm{d}X^2} = N_{\mathrm{sep}} \exp(\Phi)\operatorname{erfc}\left(\sqrt{\Phi}\right) + N_{\mathrm{emw}} \exp\left(-\Theta_{\mathrm{T}}\Phi\right)\left[1+\operatorname{erf}\left(\sqrt{\Phi/\Theta_{\mathrm{Tem}}}\right)\right] \tag{56}$$

It is however not easy to solve the equation (56) directly due to complex integrand. Further study will be performed to calculate the approximate spatial potential profile.

However, the factor γ_{e} is not arbitrarily chosen. For thermionic emission or photoemission, the γ_{e} can be regarded as constant as long as the electrode temperature or light source remains stable [48, 49], but the present research focuses on secondary electron emission where the emission coefficient is energy-dependent, and therefore closely linked with plasma properties. More precisely, the emission coefficient should be further expressed as:

$$\gamma_{\mathrm{e}} = g\left(2T_{\mathrm{ep}} + e\varphi_{\mathrm{w}}\right) \tag{57}$$

where the form of $g(x)$ in the energy range of low temperature plasma can be approximated as $g(x) = x/\varepsilon_{\mathrm{see}}$ or $g(x) = k\sqrt{x}$ [34], with $\varepsilon_{\mathrm{see}}$ and k material-dependent coefficients. For larger energy range, the SEE coefficient usually first increases with incident energy and then decreases after a certain threshold energy. Such empirical model is widely employed in a variety of plasma simulations [50, 51]. For metallic materials, the value of $\varepsilon_{\mathrm{see}}$ is usually around several decades eV [52, 53]. In practice, the situation is far more complex since the emission coefficient also depends on surface roughness, cleanness, and other local surface conditions [54, 55]. For now, only conceptual prediction is given based on the simplest form of emission coefficient: $\gamma_{\mathrm{e}} = \dfrac{2T_{\mathrm{ep}} + e\varphi_{\mathrm{w}}}{\varepsilon_{\mathrm{see}}} = \left(2+\Phi_{\mathrm{w}}\right)\Theta_{\mathrm{T}\varepsilon}$, with $\Theta_{\mathrm{T}\varepsilon} = \dfrac{T_{\mathrm{ep}}}{\varepsilon_{\mathrm{see}}}$. For cold plasma, the value of $\Theta_{\mathrm{T}\varepsilon}$ should be smaller than 1, whereas $\Theta_{\mathrm{T}\varepsilon}$ could reach or even surpasses 1 in an attached divertor of magnetically confined fusion device.

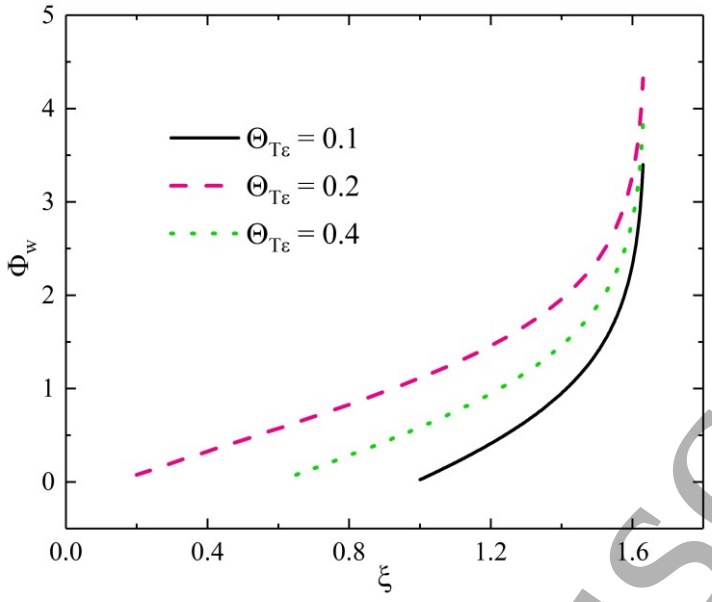

Figure 10. Calculated Φ_w considering the energy-dependent secondary electron emission coefficient.

In Figure 10 the lower bound of ξ is shifted leftwards as $\Theta_{T\varepsilon}$ increases, for the same reason in Figure 9(b). Now the γ_e increases with Φ_w and the obtained profile is somewhat shifted compared with constant γ_e case. At low Φ_w level, the incident electrons might have a larger SEE coefficient due to reflection (aka. backscattering), where the primary electron does not penetrate into the solid material but is elastically or inelastically returned. Assuming the reflection probability to be R_f, the expression of SEE coefficient has to be modified accordingly:

$$\gamma_{e,R} = R_f + (1 - R_f)\gamma_e \tag{58}$$

where $\gamma_{e,R}$ is the electron emission coefficient involving electron reflection. This is because when a reflection occurs, the "effective" SEE coefficient is 1, and if the true SEE happens, the corresponding contribution to the SEE coefficient is the non-reflection probability multiplied by the true SEE coefficient. However, the nature of such process is not as simple as described here and the coefficient R_f is also energy dependent [56].

A simple formula to estimate the reflection coefficient is based on the reflection of electron wave function by a rectangular potential well, which predicts $R_f = \left(\frac{1-\sqrt{1+\varepsilon_s/\varepsilon_{pe}}}{1+\sqrt{1+\varepsilon_s/\varepsilon_{pe}}} \right)^2$ [34]. Here $\varepsilon_s = \chi$ for dielectric, and is the sum of Fermi energy and work function for metal. ε_{pe} is the incident electron energy. The reflection coefficient is large only for low electron energy range, e.g. below 5 eV. In numerical simulations, the coefficient R_f is more commonly assumed as constant to facilitate calculation [57]. Here proof of principle study with constant backscattering coefficient is performed, shown in Figure 11. It is clear that the inclusion of reflection coefficient slightly increases Φ_w monotonously. The realistic backscattering process is however much more complex. The reflection is a 3D process though only one velocity dimension is considered here. The direction of backscattered electrons is also influenced by the electrode surface condition and roughness, potentially reducing the normal velocity component. These surface properties also change the backscattering coefficient.

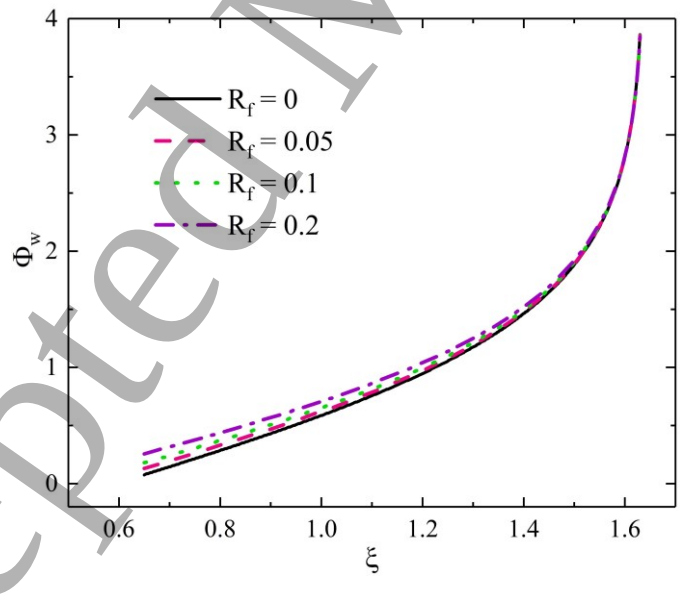

Figure 11. Calculated Φ_w considering the energy-dependent secondary electron emission coefficient and the backscattering. The factor $\Theta_{T\varepsilon} = 0.2$.

One major defect of above discussions on backscattering is the combination of secondary electron and backscattered electron in the surface emission flux term. The backscattering and secondary electron emission are completely different physical processes. The backscattered electrons usually lose a fraction of their energy when backscattered, with their VDF closely related to the plasma electron VDF at the electrode, and their effective temperature depends on both $e\varphi_{\mathrm{w}}$ and T_{ep}. The VDF of secondary electrons is however irrelevant to the plasma electron and possesses an independent temperature T_{em}. The best treatment is to separate the surface flux and reflected flux contributed by both SEE and backscattering, then rewriting equations (43) and (47), whereas the nonlinear dependence of backscattered electron temperature on $e\varphi_{\mathrm{w}}$ renders difficulty to derive analytical expression as shown from equations (48)–(50). The compromised treatment adopted in the present work aims for qualitative understanding of the influence of backscattering and better solution is expected in future works.

It is worth mentioning that the model derived above is not promptly applicable in strongly magnetized plasmas, e.g. the discharge plasma in the tokamak [48]. Firstly, the electron emission mechanism from the plasma facing components (PFCs) is more complex. Apart from secondary electron emission and the backscattering mentioned here, thermionic emission from hot PFCs and transient field emission during edge localized mode are also important. Additionally, the prompt re-decomposition of emitted electrons during initial electron gyration is crucial which depends on the sheath electric field near the surfaces. The application of proposed work in such plasma condition therefore requires more detailed investigations.

Last but not least, the influence of SEE on electron sheath can be verified experimentally by using different types of electrodes (thus different γ_{e}) biased at the same electrode potential, then checking the electron sheath properties posed by different SEE coefficients of the electrodes. Future experimental works are expected to corroborate the theoretical predictions.

5. Conclusions

The present work is dedicated to an improved understanding of electron sheath theory and its implications in plasma-surface interaction using both fluid and kinetic approaches. A fluid model considering the electron sheath entering velocity is proposed and compared to the classic electron sheath Child-Langmuir model. It is shown that the revised fluid model avoids the singularity at sheath edge in Child-Langmuir model and the latter tends to overestimate the electron sheath potential. Subsequently, a kinetic electron sheath model is constructed. Nonzero ion temperature is considered while disregarding the electron presheath structure. The kinetic model is shown to predict higher sheath potential, and the sheath size is reduced with higher ion temperatures. In the following, the electron presheath-sheath matching is developed extensively, utilizing a more realistic truncated ion distribution function due to the loss cone effect. The electron entering velocity at sheath edge is shown to be dependent on electron-ion temperature ratio and the electron sheath potential, implying a change of probe current prediction in the electron saturation region. Electron entering velocity is higher than the Bohm criterion prediction when truncated IVDF is employed. Meanwhile, attempts are made to further include the electron entering velocity into kinetic models. The exact relation between density and potential is obtained while no analytic or numerical sheath potential solution can be derived, revealing a trade-off between electron presheath structure and kinetic treatment of electron sheath. The electron sheath theory is further generalized to include the secondary electron emission on the electrode induced by sheath-accelerated plasma electrons. The *I-V* trace of applied electrode bias potential and electrode current is obtained, influenced by the boundary emission coefficient. Both constant and energy-dependent electron emission coefficient are employed in the derivation and the influence of backscattering is discussed. Further insights are also provided for future verifications of the proposed theories.

Acknowledgments

The research was conducted under the auspices of National Natural Science Foundation of China (Nos. 51827809, 52077169) and the National Key R&D Program of China (No. 2020YFC2201100).

Appendix

The following table gives the key variables adopted in derivations.

Notation	Meaning	Unit	Remarks
α_{ue0}	Normalized factor	1	$u_{e0} = \alpha_{ue0} v_{the}$
β_e	Normalized factor	1	$\Gamma_{ep,ue0} = \beta_e \Gamma_{ep,hM}$
γ_e	SEE coefficient	1	$\Gamma_{em} / \Gamma_{ep}$
$\gamma_{e,R}$	SEE coefficient	1	Consider reflection
A_c	Area of chamber wall	m^{-2}	Ion sheath presents
A_w	Area of biased electrode	m^{-2}	Electron sheath presents
Γ_{ep}	Plasma electron flux	$m^{-2}s^{-1}$	
$\Gamma_{ep,hM}$	Plasma electron flux	$m^{-2}s^{-1}$	Integrated with $f_{e,hM}$
$\Gamma_{ep,ue0}$	Plasma electron flux	$m^{-2}s^{-1}$	Integrated with $f_{e,ue0}$
Γ_i	Ion flux	$m^{-2}s^{-1}$	
Γ_{net}	Net plasma flux	$m^{-2}s^{-1}$	

Γ_{eref}	Reflected electron flux	$\mathrm{m^{-2}s^{-1}}$	
Γ_{em}	Emitted electron flux	$\mathrm{m^{-2}s^{-1}}$	
ε_0	Vacuum permittivity	$\mathrm{CV^{-1}m^{-1}}$	
$\varepsilon_{\mathrm{see}}$	SEE model factor	eV	
$f_{\mathrm{e,hM}}$	Half-Maxwellian EVDF	$\mathrm{m^{-4}s}$	
$f_{\mathrm{e,ue0}}$	Truncated EVDF	$\mathrm{m^{-4}s}$	
f_{i}	IVDF	$\mathrm{m^{-4}s}$	
E	Electric field	$\mathrm{Vm^{-1}}$	
h_{i}	Presheath density drop	1	
h_{e}	Virtual anode density drop	1	
η	Normalized potential	1	$e\left(\varphi_{\mathrm{w}}-\varphi\right)/T_{\mathrm{i}}$
η_{se}	Normalized potential	1	η at sheath edge, $e\varphi_{\mathrm{w}}/T_{\mathrm{i}}$
Θ_{T}	Temperature ratio	1	$T_{\mathrm{ep}}/T_{\mathrm{i}}$
Θ_{Tem}	Temperature ratio	1	$T_{\mathrm{em}}/T_{\mathrm{ep}}$
$\Theta_{\mathrm{T\varepsilon}}$	Temperature-energy ratio	1	$T_{\mathrm{ep}}/\varepsilon_{\mathrm{see}}$
$I\left(\eta\right)$	Normalized factor	1	$I\left(\eta\right)=0.5\left[1+\mathrm{erf}\left(\sqrt{\eta}\right)\right]$
κ	Normalized factor	1	$\exp\left(-\eta_{\mathrm{se}}\right)/2\sqrt{\pi\eta_{\mathrm{se}}}I\left(\eta_{\mathrm{se}}\right)$

Λ	Constant	1	$-\ln\left(\sqrt{2\pi}\right)$
λ_{De}	Electron Debye length	m	
μ	Ion-electron mass ratio	1	
J_{net}	Net current density	A	$e\Gamma_{\mathrm{net}}$
m_{e}	Electron mass	kg	
m_{i}	Ion mass	kg	
n_{ep}	Plasma electron density	m^{-3}	
n_{sep}	Plasma electron density	m^{-3}	Density at sheath edge
n_{em}	Emitted electron density	m^{-3}	
n_{emw}	Emitted electron density	m^{-3}	Density at biased electrode
n_{se}	Density at sheath edge	m^{-3}	
n_{i}	Ion density	m^{-3}	
N	Normalized density	1	n / n_{se}
$P_{\mathrm{e\|\|}}$	Electron parallel pressure	Pa	$n_{\mathrm{e}} T_{\mathrm{ep}}$
q_{i}	Ion heat flux	$\mathrm{Jm}^{-2}\mathrm{s}^{-1}$	
R_{f}	Reflection coefficient	1	
S_{ne}	Electron particle source	$\mathrm{m}^{-3}\mathrm{s}^{-1}$	

S_{ni}	Ion particle source	$m^{-3}s^{-1}$	
S_{me}	Electron momentum source	$kgm^{-2}s^{-2}$	
S_{mi}	Ion momentum source	$kgm^{-2}s^{-2}$	
T_{ep}	Plasma electron temperature	eV	
T_{em}	Emitted electron temperature	eV	
T_i	Ion temperature	eV	
u_{e0}	Electron entering velocity	ms^{-1}	Velocity at sheath edge
u_e	Electron fluid velocity	ms^{-1}	
u_i	Ion fluid velocity	ms^{-1}	
v_{icut}	Ion cutoff velocity	ms^{-1}	$\sqrt{2\eta}v_{thi}$
v_{ecut}	Electron cutoff velocity	ms^{-1}	$\sqrt{2\Phi_w}v_{the}$
v_{the}	Electron thermal velocity	ms^{-1}	$\sqrt{T_{ep}/m_e}$
v_{thi}	Ion thermal velocity	ms^{-1}	$\sqrt{T_i/m_i}$
φ_{esh}	Electron sheath potential	V	Positive
φ_{ish}	Ion sheath potential	V	Negative
φ_w	Biased electrode potential	V	Positive
Φ	Normalized potential	1	$e\varphi/T_{ep}$

Φ_w	Normalized potential	1	$e\varphi_w / T_{ep}$
ξ	Normalized factor	1	$\Gamma_{net}/(n_{se}\sqrt{2T_{em}/\pi m_e})$
x_{ish}	Ion sheath size	m	
x_{esh}	Electron sheath size	m	
X	Normalized position	1	x/λ_{De}

References

[1] Buchenauer D *et al* 1995 *Rev. Sci. Instrum.* **66** 827

[2] Li H L and Sun A B 2021 *Comput. Phys. Commun.* **259** 107629

[3] Das G C, Deka R and Bora M P 2016 *Phys. Plasmas* **23** 042308

[4] Février O *et al* 2018 *Rev. Sci. Instrum.* **89** 053502

[5] Robertson S 2013 *Plasma Phys. Control. Fusion* **55** 093001

[6] Han J *et al* 2020 *Phys. Plasmas* **27** 063509

[7] Zhou X Y *et al* 2021 *Plasma Sci. Technol.* **23** 064003

[8] Zhao K *et al* 2021 *Plasma Sci. Technol.* **23** 115404

[9] Ding Z *et al* 2021 *Plasma Sci. Technol.* **23** 095403

[10] Hershkowitz N 2005 *Phys. Plasmas* **12** 055502

[11] Jin C *et al* 2022 *Plasma Sci. Technol.* **24** 025404

[12] Franklin R N 2003 *J. Phys. D: Appl. Phys.* **36** R309

[13] Baalrud S D, Hershkowitz N and Longmier B 2007 *Phys. Plasmas* **14** 042109

[14] Richards B *et al* 1994 *Phys. Plasmas* **1** 1606

[15] Law D A *et al* 1998 *Phys. Rev. Lett.* **80** 4189

[16] Singh N and Jaggernauth A 1996 *J. Geophys. Res.* **101** 17229

[17] Fetterman A J, Raitses Y and Keidar M 2008 *Carbon* **46** 1322

[18] Medicus G 1961 *J. Appl. Phys.* **32** 2512

[19] Yee B T *et al* 2017 *Plasma Sources Sci. Technol.* **26** 025009

[20] Scheiner B *et al* 2015 *Phys. Plasmas* **22** 123520

[21] Stenzel R L *et al* 2011 *Phys. Plasmas* **18** 062113

[22] Stenzel R L *et al* 2011 *Phys. Plasmas* **18** 062112

[23] Scheiner B *et al* 2016 *Phys. Plasmas* **23** 083510

[24] Hood R *et al* 2016 *Phys. Plasmas* **23** 113503

[25] Takamura S *et al* 2004 *Contrib. Plasma Phys.* **44** 126

[26] Baalrud S D *et al* 2020 *Plasma Sources Sci. Technol.* **29** 053001

[27] Lafleur T 2021 *Plasma Sources Sci. Technol.* **30** 055018

[28] Chen X C *et al* 2021 *Plasma Sources Sci. Technol.* **30** 065002

[29] Loizu J *et al* 2012 *Phys. Plasmas* **19** 083507

[30] Riemann K U 1991 *J. Phys. D: Appl. Phys.* **24** 493

[31] Kaganovich I D *et al* 2007 *Phys. Plasmas* **14** 057104

[32] Sheehan J P *et al* 2014 *Phys. Plasmas* **21** 063502

[33] Sheehan J P *et al* 2013 *Phys. Rev. Lett.* **111** 075002

[34] Sun G Y *et al* 2019 *Plasma Sources Sci. Technol.* **28** 055001

[35] Loizu J, Ricci P and Theiler C 2011 *Phys. Rev. E* **83** 016406

[36] Stangeby P C 2000 *Plasma Phys. Control. Fusion* **42** B271

[37] Moritz J *et al* 2021 *Phys. Plasmas* **28** 083501

[38] Faudot E *et al* 2013 *Phys. Plasmas* **20** 043514

[39] Langendorf S and Walker M 2015 *Phys. Plasmas* **22** 033515

[40] Sun G Y, Sun A B and Zhang G J 2020 *Phys. Rev. E* **101** 033203

[41] Uhm H S, Choi E H and Cho G S 2009 *Appl. Phys. Lett.* **94** 031501

[42] Rösler M and Brauer W 1981 *Phys. Status Solidi* **104** 161

[43] Zhang S *et al* 2021 *Plasma Sources Sci. Technol.* **30** 055007

[44] Sun G Y *et al* 2019 *Plasma Process. Polym.* **16** 1900093

[45] Sun J Y *et al* 2019 *Phys. Plasmas* **26** 063505

[46] Campanell M D 2013 *Phys. Rev. E* **88** 033103

[47] Qing S W and Hu Z 2017 *AIP Adv.* **7** 085220

[48] Tolias P *et al* 2020 *Nucl. Mater. Energy* **25** 100818

[49] Dove A *et al* 2012 *Phys. Plasmas* **19** 043502

[50] Schwarz S A 1990 *J. Appl. Phys.* **68** 2382

[51] Furman M A and Pivi M T F 2002 *Phys. Rev. ST Accel. Beams* **5** 124404

[52] Oyarzabal E, Martin-Rojo A B and Tabarés F L 2014 *J. Nucl. Mater.* **452** 37

[53] Song B P *et al* 2016 *Appl. Surf. Sci.* **390** 346

[54] Demidov V I *et al* 2015 *Phys. Plasmas* **22** 104501

[55] Zhou R D *et al* 2019 *J. Phys. D: Appl. Phys.* **52** 375304

[56] Cimino R *et al* 2004 *Phys. Rev. Lett.* **93** 014801

[57] Vaughan R M 1993 *IEEE Trans. Electron Dev.* **40** 830